



Chance-Constraint-Based Design of Open-Loop Controllers for Linear Uncertain Systems

Souransu Nandi D., Student Member, IEEE, and Tarunraj Singh D., Senior Member, IEEE

Abstract—This paper considers the problem of state-tostate transition with state and control constraints, for a linear system with time-invariant model parameter uncertainties. Polynomial chaos is used to transform the stochastic model to a deterministic surrogate model. This surrogate model is used to pose a chance-constrained optimal control problem where the state constraints and the residual energy cost are represented in terms of the mean and variance of the stochastic states. The resulting convex optimization problem is numerically illustrated on the problem of rest-to-rest maneuver of the benchmark floating oscillator and on an experimental two-tank setup.

Index Terms—Chance constraint, polynomial chaos (PC), stochastic optimal control, uncertain system, vibration control.

I. INTRODUCTION

ESIGNING control strategies under assumptions of uncertainties in the model has been a topic of research interest for many years and a number of researchers have made contributions to the field [1], [2], and [3]. Such robust control techniques find applications spread across various domains in engineering. Mechatronic applications such as nanopositioning devices such as scanning probe microscope, wafer scanners, atomic force microscopes, and scanning electron microscopes, require precise positioning for their optimal performance [2], [4]. Some other applications which have shown benefits from the design of robust open-loop control for vibration suppression include industrial robots [5], and even water level control for an industrial boiler unit (with parameter uncertainties) [6] among many others.

One of the open-loop approaches of dealing with model parameter uncertainty is input shaping which reduces the sensitivity of the cost function in the proximity of the nominal model by forcing the local sensitivity to zero [1], [7]. The other popular approach has been to design controllers so as to take care of worst case scenarios [8]. But this method can often lead to very conservative results which may not be practical.

Manuscript received October 2, 2017; revised January 4, 2018 and March 23, 2018; accepted May 19, 2018. Date of publication May 24, 2018; date of current version August 14, 2018. This work was supported by NSF under Award CMMI-1537210. (Corresponding author: Tarunraj Singh.)

The authors are with the Mechanical and Aerospace Engineering, University at Buffalo, Buffalo, NY 14260 USA (e-mail: souransu@ buffalo.edu; tsingh@buffalo.edu).

Color versions of one or more of the figures in this paper are available online at http://ieeexplore.ieee.org.

Digital Object Identifier 10.1109/TMECH.2018.2840107

A way to mitigate the issues of both these methods is to use the information available in the probability distributions of the uncertain variables to address robustness. In doing so, it often leads to posing the optimization problems (i.e., optimal control problems) with probabilistic or chance constraints (see [9]-[11]). These chance constraints can in fact be written as deterministic constraints to solve the optimization problem. For example, Calafiore and El Ghaoui [12] investigate linear chance constraints which are robust to the distribution of the random variables (r.v.). Their approach allows one to write any linear chance constraint as a deterministic constraint based on the available r.v. parameters such as mean, variance, and support.

Mesbah et al. in [13] present a generic framework for implementing linear chance inequality constraints in model predictive control (MPC) for nonlinear systems with parametric uncertainties. Polynomial chaos (PC) which was first investigated by Norbert Wiener in [14], for Gaussian processes and was generalized by Xiu et al. [15] was used to determine the first two moments of the stochastic states which are then used to enforce these chance constraints. However, the nonlinear inequality constraints remain deterministic and are limited to the nominal trajectories of the states. The cost in the MPC framework is also considered to be nonprobabilistic.

In this paper, the focus is on linear systems with linear constraints and a residual energy cost which has a quadratic form, making the entire problem convex in a deterministic framework. In a probabilistic framework, most often, the worst case state trajectories have significantly low associated probabilities of realization [16]. It is also common knowledge that one needs to tradeoff a performance for robustness when dealing with the uncertain systems. Consequently, considering a probabilistic cost function permits a simple approach for the tradeoff analysis. The chance constraint corresponding to a linear constraint for an uncertain system results in a cone constraint, but does not permit posing a quadratic cost using the same framework. This prompts using a linear approximation of the quadratic cost, which permits using the chance constraint to pose a convex optimization problem for the design of controllers. Although the individual ideas of representing stochastic states using the PC expansion, the linear approximation of l_2 norm and chance-constrainedbased optimization is not new, the novelty of this paper lies in the fluid integration of the three frameworks resulting in a convex optimization framework. The flowchart presented in Fig. 1 encapsulates the sequential exercise of various conceptual components that lead to the chance-constrained problem formulation. The flowchart also includes the section titles which can

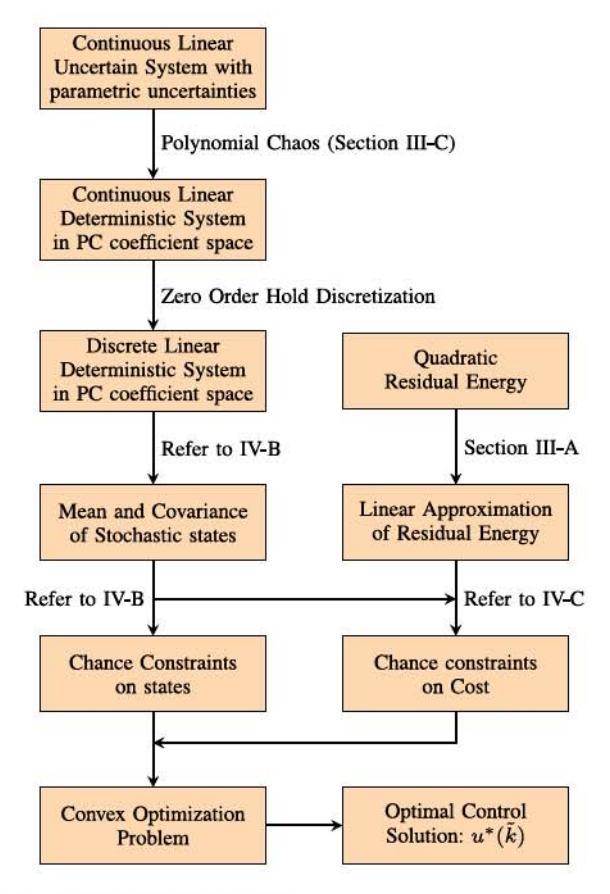


Fig. 1. Flowchart of the algorithm.

help the reader visualize how the disparate algorithms/concepts are integrated.

The structure of the paper is as follows. Section II defines the mathematical optimization problem whose solution is being sought. Section III presents details about the proposed technique to solve the optimization problems. Section IV presents the Wie and Bernstein [17] benchmark problem which has been selected to illustrate the proposed method. Finally, the paper is completed with the experimental results on a two tank system in Section V and concluding remarks in Section VI.

II. PROBLEM STATEMENT

This section of the paper describes the formulation of a optimization problem to design the controllers for the point-to-point maneuvers of the spring-mass-dashpot class of systems. Euler–Lagrange equations for the linear mechanical systems can be represented as the vector second-order models

$$M\ddot{z} + C\dot{z} + Kz = Du \tag{1}$$

where M,C,K, and D are mass, damping, stiffness, and control influence matrices, respectively; the energy (E) in the system at any time instant is

$$E = \frac{1}{2}\dot{z}^T M \dot{z} + \frac{1}{2}z^T K z. \tag{2}$$

A state-space representation of the system is given by

$$\underbrace{\left\{\frac{\dot{z}}{\ddot{z}}\right\}}_{\dot{z}} = \underbrace{\begin{bmatrix}\mathbf{0} & I\\ -M^{-1}K & -M^{-1}C\end{bmatrix}}_{A'}\underbrace{\left\{\frac{z}{\dot{z}}\right\}}_{Z} + \underbrace{\begin{bmatrix}\mathbf{0}\\ M^{-1}D\end{bmatrix}}_{B'}u \quad (3)$$

where A' is the state matrix and B' is the control influence matrix of the continuous time system. Assuming $z \in \mathbb{R}^n$ (i.e., $z = [z_1, \ldots, z_n]^T$), $Z \in \mathbb{R}^{2n}$. The discrete-time representation of (3) is

$$Z\left(\tilde{k}+1\right) = AZ\left(\tilde{k}\right) + Bu\left(\tilde{k}\right) \tag{4}$$

which will be used for the controller design, where \tilde{k} represents the \tilde{k} th time-step. The control objective is to determine $u(\tilde{k})$ which can be used to drive the system from an initial state (Z(0)) at time t=0 to a final desired state $(Z_d(T_f))$ at time $t=T_f$ with constraints on the states and control input during the transition. However, since the system is considered to have parametric uncertainties, it is impossible to find an open-loop control $u(\tilde{k})$ which assures all the realizations of the dynamic system reach $Z_d(T_f)$. To make all the realizations reach as close to the desired value as possible, a quantity of measure is necessary which characterizes this closeness. A popular choice for this quantity in the literature has been the residual energy (and thus, the same is chosen for this paper).

The residual energy (excursion from the desired terminal energy) is defined as $E_r(T_f) = \frac{1}{2}\dot{x}^TM\dot{x} + \frac{1}{2}x^TKx$, where the residual states are defined by

$$X = \begin{bmatrix} x(T_f) \\ \dot{x}(T_f) \end{bmatrix} = Z(T_f) - Z_d(T_f). \tag{5}$$

 $Z(T_f)$ is the terminal value of the states of any realization of the model in (4). Note that, K is singular when the system includes a rigid body mode. In such a scenario, a pseudoenergy function [8] is included to ensure that E_r is positive definite.

Equation (4) can also be written as a linear function of only the control inputs and the initial conditions as

$$Z(\tilde{k}+1) = A^{\tilde{k}}Z(0) + \sum_{i=0}^{\tilde{k}} A^{\tilde{k}-i}Bu(i).$$
 (6)

This linear mapping can then be used to write the state constraints at any instant in time (and if need be at all instants in time i.e., $\forall \tilde{k}$) with the help of an appropriate output matrix.

Finally, the optimal control problem (P1) of interest can be posed as

minimize_{m{u}}
$$E_r$$
 subject to $u_{lb}\leqslant u\left(\tilde{k}\right)\leqslant u_{ub} \quad \forall \tilde{k}$
$$\Gamma Z\left(\tilde{k}\right)\leq \Phi \qquad \forall \tilde{k} \tag{7}$$

where Γ is an output matrix and Φ is the output constraint. However, E_r is a r.v. and therefore (P1) needs to be rewritten in a more meaningful way. A popular approach in the literature has been to seek the worst case (minimax) solution to (P1). The minimax optimal control problem (P2) can be posed as

$$\begin{array}{ll} \text{minimize}_{\boldsymbol{u},f} & f \\ \\ \text{subject to} & E_r^{(i)} \leqslant f & \forall i=1,\dots,p \\ \\ & u_{lb} \leqslant u\left(\tilde{k}\right) \leqslant u_{ub}, & \forall \tilde{k} \\ \\ & \Gamma Z\left(\tilde{k}\right) \leq \Phi & \forall \tilde{k} \end{array} \tag{8}$$

where f (cost function) represents the upper bound on the residual energy E_r and p represents the number of different realizations of the uncertain system. These realizations could be generated using Monte Carlo (MC), latin hypercube, or any other sampling approaches. If the state constraints are linear, then the optimization problem can be shown to be convex.

Since there lies motivation to incorporate information present in the probabilities of the states into the control design, two more optimal control problems can be posed where the state constraints and the energy constraints in problem (P2) are probabilistic. The stochastic optimal control problem where only the state constraints are probabilistic (P3) is posed as

minimize
$$_{oldsymbol{u},f}$$
 f subject to $E_r^{(i)} \leqslant f$ $\forall i=1,\ldots,p$ $u_{lb} \leqslant u\left(\tilde{k}\right) \leqslant u_{ub},$ $\forall \tilde{k}$ $P\left(\Gamma Z\left(\tilde{k}\right) \leq \Phi\right) \geq 1-\epsilon_1$ $\forall \tilde{k}$ (9)

where P(W) represents the probability with which event W occurs and ϵ_1 represents the risk level for the state constraint. Similarly, the stochastic optimal control problem where the state constraints as well as the energy constraints are probabilistic (P4) is posed as

$$\begin{array}{ll} \text{minimize}_{u,f} & f \\ \text{subject to} & P(E_r \leqslant f) \geq 1 - \epsilon_2 \\ & u_{lb} \leqslant u\left(\tilde{k}\right) \leqslant u_{ub}, \qquad \forall \tilde{k} \\ & P\left(\Gamma Z\left(\tilde{k}\right) \leq \Phi\right) \geq 1 - \epsilon_1 \quad \forall \tilde{k} \end{array} \tag{10}$$

and ϵ_2 represents the risk level for the energy constraint. This paper is aimed at presenting an algorithm to solve (P3) and (P4).

III. CONTROLLER DESIGN

This section presents details on the methodology being used to solve (P3) and (P4) and has been divided into subsections to explain various parts of the process. Section III-A summarizes ways to approximate the quadratic residual energy by a set of linear functions. Section III-B presents the manner in which a linear chance constraint can be written as a nonprobabilistic cone constraint. Section III-C gives a short overview of the PC and shows its application in estimating the moments of the stochastic states.

A. Linear Approximation of the Residual Energy

The residual energy (which is a quadratic function of the residual states) can be approximated by a linear function of a new set of states defined by

$$Y = \frac{1}{\sqrt{2}} \underbrace{\begin{bmatrix} \sqrt{K} & \mathbf{0} \\ \mathbf{0} & \sqrt{M} \end{bmatrix}}_{L} X. \tag{11}$$

In Y space, E_r represents a hypersphere (since $E_r = Y^T Y$). The idea is to approximate this hypersphere with a set of hyperplanes such that the volume enclosed by the hyperplanes would be circumscribed by the hypersphere. This idea was first developed in [18] where a systematic method was presented in generating the necessary hyperplanes for approximating a hypersphere in any dimension. Theoretically it would need an infinite number of hyperplanes to exactly reproduce a hypersphere. However, for implementation only a finite number of them are used. The number of hyperplanes generated, therefore, depends on the level of approximation desired.

For example, the most basic approximation (a.k.a. a Level 0 approximation) of the space $(E_r \leq f)$ would simply be given by the intersection of the half-spaces described by

$$||Y||_1 \le f. \tag{12}$$

If $Y \in \mathbb{R}^{\tilde{n}}$ (i.e., $Y = [y_1, \dots, y_{\tilde{n}}]^T$), (12) is equivalent to the convex space formed from the intersection of the $2^{\tilde{n}}$ half-spaces bounded by the $2^{\tilde{n}}$ hyperplanes

$$\pm y_1 \pm y_2 \dots \pm y_{\tilde{n}} = f. \tag{13}$$

Similarly, [18] allows one to determine higher Level approximations to the space enclosed within the E_r hypersphere. Fig. 2 illustrates the first octant for three different Levels of approximation for a three dimensional (3-D) hypersphere.

An alternative to approximating the E_r hypersphere is to substitute it by another relevant geometric shape made from hyperplanes. One such example would be to use a cube. The cube can be described by the intersection of the half-spaces

$$||Y||_{\infty} \le f \tag{14}$$

which is equivalent to $2\tilde{n}$ half-spaces bounded by $2\tilde{n}$ planes

$$-f \le y_i \le f \qquad \forall i = 1 \dots \tilde{n}.$$
 (15)

It should also be pointed out that for spring-mass-dashpot class of systems, $\tilde{n}=2n$.

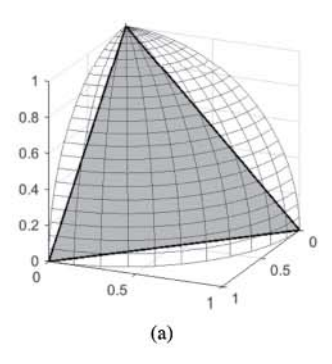
B. Implementation of Probabilistic Constraints

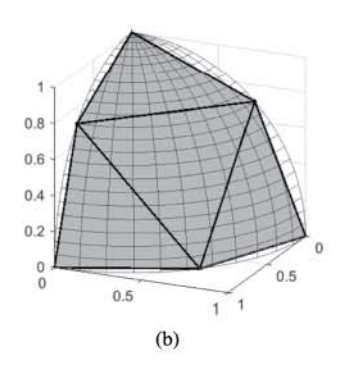
As alluded to previously, [12] provides an approach to rewrite the linear probabilistic inequalities as the nonprobabilistic inequalities. In their work, they prove that if a and b are r.v. with known means and variances, then the constraint

$$\operatorname{Prob}\left\{a^{T}x + b \le 0\right\} \ge 1 - \epsilon \tag{16}$$

can be conservatively approximated with the constraint

$$\sqrt{\frac{1-\epsilon}{\epsilon}} \left\{ \operatorname{var} \left[a^T x + b \right] \right\}^{1/2} + E \left[a^T x + b \right] \le 0 \tag{17}$$





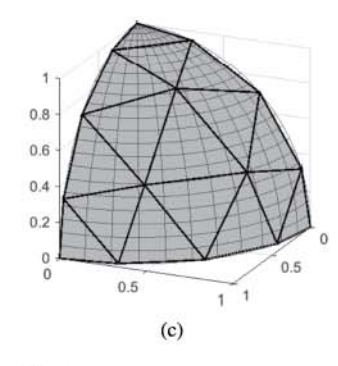


Fig. 2. (a) Level 0 approximation for $\tilde{n}=3$. (b) Level 1 approximation for $\tilde{n}=3$. (c) Level 2 approximation for $\tilde{n}=3$.

where ϵ represents the risk level i.e., the probability with which the constraint is permitted to be violated. It should be noted that the constraint is conservative since it subsumes all distributions with the same mean and variance. This means that the equality sign of (16) is going to be active for only a particular distribution (which is unknown).

Therefore, this simple formulation now allows us to enforce the linear probabilistic constraints as long as the mean and the variance of the r.v. are known.

C. Uncertainty Quantification Using the PC

This section presents a tool which allows one to characterize the evolution of the uncertainty for the stochastic systems by expressing the stochastic states as a polynomial function of the uncertain parameters of the model and determine the mean and variance that are needed for implementing the chance constraints.

Let a stochastic linear dynamical system be expressed in the form

$$\dot{x}(t,\xi) = A(\xi)x(t) + B(\xi)u(t)$$
 and $x(t_0,\xi) = x_0$ (18)

where, $x \in \mathbb{R}^{\tilde{n}}$ is the state vector, $\xi \in \mathbb{R}^m$ is the vector of r.v. with known probability density function (pdf), and u(t) is the control input.

From generalized polynomial chaos (gPC) theory, the states can be expressed as

$$x(t,\xi) = \sum_{i=0}^{\infty} x_{:,i}(t) \Psi_i(\xi)$$
 (19)

where, $\Psi_i(\xi)$ is a complete set of multivariate orthogonal (w.r.t. the pdf of ξ) polynomials and $x_{:,i} \in \mathbb{R}^{\bar{n}}$ is the time varying coefficient vector (i.e., $x_{:,i} = [x_{1,i} \ldots x_{\bar{n},i}]^T)$ of $\Psi_i(\xi)$. The selection of the set of orthogonal polynomials $(\Psi_i(\xi))$ for popular distributions is given by the Wiener–Askey scheme [15]. For other general distributions, a set of corresponding orthogonal polynomials can also be generated via the Gram–Schmidt orthogonalization method.

As an approximation, the expansion is usually truncated to a finite number of terms (depending on the desired accuracy) [15]. Hence, (19) is rewritten as

$$x(t,\xi) pprox \sum_{i=0}^{N} x_{:,i}(t) \Psi_i(\xi).$$
 (20)

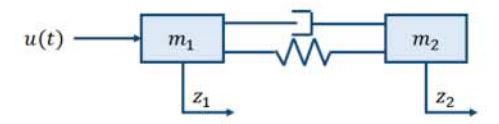


Fig. 3. Two Mass-Spring-Damper System.

The objective is to evaluate the unknown vectors $x_{:,i}(t)$ over time. Equation (20) is substituted in (18) to get

$$\sum_{i=0}^{N} \dot{x}_{:,i}(t)\Psi_i(\xi) = A(\xi) \left[\sum_{i=0}^{N} x_{:,i}(t)\Psi_i(\xi) \right] + B(\xi)u(t).$$
(21)

Galerkin projection is then exercised on (21) over each of the orthogonal basis functions (i.e., Ψ_j , where $j=0,1,\ldots,N$) to get a set of deterministic differential equations for the coefficients $x_{:,i}$. The solution to these equations yield the sought elements of $x_{:,i}(t)$. The desired moments (such as mean and variance) of the stochastic states $x(t,\xi)$ can subsequently be calculated from $x_{:,i}(t)$, completing the final piece of the puzzle. A more detailed implementation for the Galerkin projection can be found in [19].

Once the mean and variance are known, chance energy constraints as well as the chance state constraints can be imposed. As a result, the optimization problems (P3) and (P4) can now be solved using any convex programming solver.

IV. SIMULATED EXAMPLE PROBLEM

This section uses the benchmark two mass floating oscillator (see Fig. 3) to illustrate the solutions catering to the (P2), (P3), and (P4) problems.

The M, C, K, and D matrices corresponding to the oscillator are given by

$$M = \begin{bmatrix} 5 & 0 \\ 0 & 5 \end{bmatrix}; C = \begin{bmatrix} c & -c \\ -c & c \end{bmatrix}; K = \begin{bmatrix} k & -k \\ -k & k \end{bmatrix}$$
 (22)

and
$$D = [1, 0]^T$$
.

It is assumed that k and c are uncertain. The control objective in this example is to find the control trajectory $u(\tilde{k})$ which can move the system from an initial rest state $Z(0) = [0,0,0,0]^T$ to a final desired rest state $Z_d(T_f) = [1,1,0,0]^T$ under the control

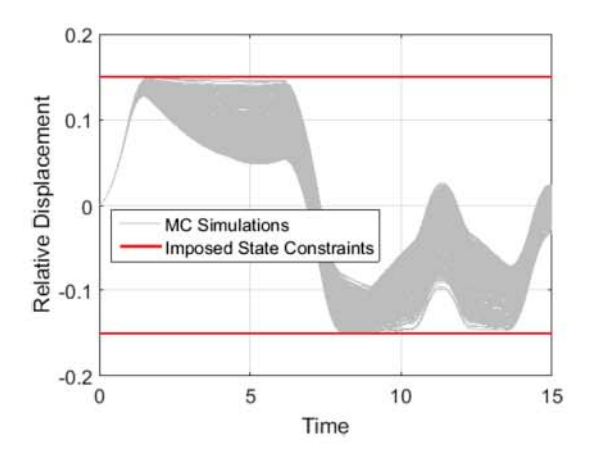


Fig. 4. Relative displacement versus time for nonprobabilistic state constraint.

constraints

$$\left|u\left(\tilde{k}\right)\right| \le 1 \quad \forall \ \tilde{k}$$
 (23)

and the state constraints

$$\left|z_1\left(\tilde{k}\right) - z_2\left(\tilde{k}\right)\right| \le 0.15 \quad \forall \, \tilde{k}.$$
 (24)

All simulations in this paper were done with $T_f = 15$. The sampling time for discretization used was $T_s = 0.1$. Therefore the total number of steps were $N_t = T_f/T_s + 1 = 151$.

A. Minimax Solution

This section presents the results for the case when both the energy and state constraints are nonprobabilistic. This basically comprises solving the optimal control problem (P2), corresponding to a minimax problem where the maximum residual energy over the domain of uncertain variables is minimized. The variables k and c are assumed to be uniformly distributed with the distributions: $k \in U[0.7, 1.3]$ and $c \in U[0.8, 1.2]$, respectively. In this example, uniformly gridding the domain of the two uncertain variables into 21 points each results in 21² distinct realizations of k and c. This results in $p = 21^2$ constraints at any time which can include the energy (terminal time) and state constraints (all sampling times). It should be noted that gridding the uncertain space guarantees the satisfaction of the constraints only at the grid points. For illustration, the residual energy which is a quadratic function of the system states, is chosen as the cost function. MC simulations of the dynamic system with the obtained control solution and the resulting relative displacement of the masses for all the realizations are shown in Fig. 4.

It is evident from the figure that the relative displacements (in this case) always lies (i.e., at all times) within the imposed state constraint bounds indicated by the solid red lines (even though the constraints were imposed only at the grid points).

B. Probabilistic State Constrained Solution

This section is used to present results for the floating oscillator maneuver when the optimization problem (P3) is solved.

To illustrate that different probability distributions yield different results, three separate distributions with same means (E[k] = 1, E[c] = 1) and variances $(\sigma^2[k] = 0.018, \sigma^2[c] = 0.008)$ for k and c in the example problem are considered. Note that E[.] refers to the expectation operation and $\sigma^2[.]$ refers to the variance.

The first case is for the uniform distributions and is defined in terms of two independent r.v. ξ_{u1} and ξ_{u2} (where $\xi_{u1}, \xi_{u2} \in U[-1, 1]$). Therefore, we have

$$k = 1 + 0.2324\xi_{u1}$$
 and $c = 1 + 0.1549\xi_{u2}$. (25)

The second case is for beta distributions and is defined via two independent beta distributed r.v. ξ_{b1} and ξ_{b2} (where $\xi_{b1}, \xi_{b2} \in [-1,1]$) with the distribution parameters a=1 and b=1. Therefore, we get

$$k = 1 + 0.3\xi_{b1}$$
 and $c = 1 + 0.2\xi_{b2}$. (26)

The r.v. for the final case (ξ_{m1}, ξ_{m2}) is chosen from the work in [20]. $\xi_{m1}, \xi_{m2} \in [-1, 1]$, are independent and have marginal pdfs given by

$$p(\xi_{mj}) = 1 - W \sum_{i=0}^{1} A_i |\xi_{mj}|^{2-i+1}, \text{ for } j = 1, 2$$
 (27)

where W=-(3)!, $A_i=\frac{(-1)^{i\,1}C_i}{2-i+1},$ and $^1C_i=\frac{1!}{i!(1-i)!}.$ k and c are written in terms of $\xi_{m\,1}$ and $\xi_{m\,2}$ as

$$k = 1 + 0.3674\xi_{m1}$$
 and $c = 1 + 0.2449\xi_{m2}$. (28)

Since posing the chance constraints requires the mean and the variance, the first step at this point is to obtain a PC expansion of the stochastic model.

Development of the PC model is shown only with respect to the uniform distribution case; the PC coefficients for the other distributions can be evaluated in an identical fashion.

The orthogonal basis functions $\Psi_i(\xi)$ for a uniform distribution are the Legendre polynomials. Since there are a couple of uncertain parameters, 2-D Legendre polynomials (derived from a tensor product of 1-D Legendre polynomials) form the basis functions.

The basis functions $\Psi_i(\xi)$ where $\xi = [\xi_{u1}, \xi_{u2}]^T$ are derived from the tensor product of the first six Legendre polynomials in ξ_{u1} and ξ_{u2} . (The choice of six is chosen as a compromise between the level of accuracy desired and computational expense.) This leads to a total of $6^2 = 36$ basis functions (i.e., N = 35). Using the Galerkin approach and recognizing that for the example $\tilde{n} = 2n = 4$, $(N+1)\tilde{n} = 144$ deterministic equations are formed which are used to evaluate the PC coefficients. Therefore, if the states are expanded as

$$Z = \begin{bmatrix} Z_1 \\ Z_2 \\ Z_3 \\ Z_4 \end{bmatrix} = \begin{bmatrix} Z_{1,0} \\ Z_{2,0} \\ Z_{3,0} \\ Z_{4,0} \end{bmatrix} \Psi_0 + \begin{bmatrix} Z_{1,1} \\ Z_{2,1} \\ Z_{3,1} \\ Z_{4,1} \end{bmatrix} \Psi_1 + \dots + \begin{bmatrix} Z_{1,35} \\ Z_{2,35} \\ Z_{3,35} \\ Z_{4,35} \end{bmatrix} \Psi_{35}$$
(29)

where $Z = [z_1, z_2, \dot{z_1}, \dot{z_2}]^T$ then the deterministic equations formed are given by

$$\begin{bmatrix} \dot{Z}_{1,0}\langle \Psi_0, \Psi_0 \rangle \\ \vdots \\ \dot{Z}_{4,35}\langle \Psi_{35}, \Psi_{35} \rangle \end{bmatrix} = G \begin{bmatrix} Z_{1,0} \\ \vdots \\ Z_{4,35} \end{bmatrix} + Hu$$
 (30)

where $\langle p(\xi), q(\xi) \rangle$ is the inner product equal to $\int p(\xi) q(\xi) p df(\xi) d\xi$, G and H are matrices determined from the Galerkin projection.

Equation (30) can be solved to determine the coefficients $Z_{1,0}$ through $Z_{4,35}$. Consequently, all the moments of the states can then be determined from these coefficients. Our studies confirm the assessment of Kim $et\ al.$ [21] that the mean and variance can be computed accurately with the low-order PC expansion. Since, the proposed chance-constrained optimization only requires the mean and variance, the gPC serves as a computationally efficient tool for estimating them.

Moreover, since the control problem has been posed in the discrete domain, (30) is discretized as

$$Z_{C}\left(\tilde{k}+1\right) = \bar{A}Z_{C}\left(\tilde{k}\right) + \bar{B}u\left(\tilde{k}\right) \tag{31}$$

where $Z_C = [Z_{1,0}, \dots, Z_{1,35}, Z_{2,0}, \dots, Z_{3,0}, \dots, Z_{4,35}]^T$. A similar development for any distribution of k and c can be made.

The PC expansions for each of these three cases are used to determine the mean and the variance of the states at each time instant. Then these means and variances are used to implement a probabilistic state constraint where the probabilistic state constraint is written in the form of (17). In this section, the optimal control problem (P3) is chosen to be solved with a Level 0 approximation of the residual energy for the example problem. A linear version of the residual energy need not be chosen though and any of the other formulations are acceptable. The control constraints are the same as (23). The relative displacement state constraint is however modified to the probabilistic constraints

$$\operatorname{Prob}\left\{Z_{1}\left(\tilde{k}\right)-Z_{2}\left(\tilde{k}\right)-0.15\leq0\right\}\geq1-\epsilon_{1}\qquad(32)$$

$$\operatorname{Prob}\left\{-Z_{1}\left(\tilde{k}\right)+Z_{2}\left(\tilde{k}\right)-0.15\leq0\right\}\geq1-\epsilon_{1}\tag{33}$$

 $\forall \tilde{k}$. Equation (32) is equivalent to

$$k_e \{ \text{var} [Z_1 - Z_2 - 0.15] \}^{1/2} + E[Z_1 - Z_2 - 0.15] \le 0$$
 (34)

where $k_e = \sqrt{\frac{1-\epsilon_1}{\epsilon_1}}$. If a vector is defined as $C_{\rm con} = [1,-1,0,0]^T$, then the constraint can be simplified to

$$k_e \left\{ \operatorname{var} \left[C_{\operatorname{con}}^T Z \left(\tilde{k} \right) - 0.15 \right] \right\}^{1/2} + E \left[C_{\operatorname{con}}^T Z \left(\tilde{k} \right) - 0.15 \right] \le 0.$$
(35)

 $Z(\tilde{k})$ can be represented as a linear function of the control input as

$$Z\left(\tilde{k}\right) = \Psi A_{eq}\left(\tilde{k}\right)U\tag{36}$$

where

$$\underbrace{\Psi}_{(\bar{n}\times\bar{n}(N+1))} = \begin{bmatrix} \Psi_0 & \dots & \Psi_N & & \mathbf{0} \\ & & \ddots & & \\ \mathbf{0} & & \Psi_0 & \dots & \Psi_N \end{bmatrix} \tag{37}$$

$$\underbrace{A_{eq}\left(\tilde{k}\right)}_{\left(\tilde{n}\left(N+1\right)\times N_{t}\right)} = \begin{bmatrix} \bar{A}^{\tilde{k}-1}\bar{B} & \bar{A}^{\tilde{k}-2}\bar{B} & \dots & \bar{B} & 0^{T} \end{bmatrix}$$
(38)

and $U = [u(0), \ldots, u(\tilde{k}), \ldots, u(150)]^T$. The last column of $A_{eq}(\tilde{k})$ is a null matrix whose dimension is $\tilde{n}(N+1) \times N_t - \tilde{k} + 1$. This null matrix shows that control input at the time instants greater than \tilde{k} do not influence the states at \tilde{k} . One must be aware that Z_C in (31) is basically $Z_C(\tilde{k}) = A_{eq}(\tilde{k})U$.

It should be noted that Ψ is different for the three distinct cases. The basis functions (Ψ_0 through Ψ_N) for the first case are 2-D Legendre polynomials. The basis functions for the second case are 2-D Jacobi polynomials and the basis functions for the final case are generated using the Gram–Schmidt orthogonalization. Therefore, different values of \bar{A} , \bar{B} , A_{eq} , and Ψ are calculated for each distribution. However, the order of the PC is chosen to be N=35 to be the same for all the three cases. Now, using (36) we get

$$E\left[C_{\text{con}}^{T}Z\left(\tilde{k}\right)-0.15\right]=C_{\text{con}}^{T}E\left[\Psi A_{eq}\left(\tilde{k}\right)U\right]-0.15.$$
(39)

Since, the only r.v. is Ψ , the equation reduces to

$$E\left[C_{\text{con}}^{T}Z\left(\tilde{k}\right)-0.15\right]=C_{\text{con}}^{T}E[\Psi]A_{eq}\left(\tilde{k}\right)U-0.15. \tag{40}$$

Similarly, $\text{var}[C_{\text{con}}^T Z(\tilde{k}) - 0.15]$ can be reduced to

$$U^{T} A_{eq}^{T} \underbrace{\left(E \left[\Psi^{T} C_{\mathsf{con}} C_{\mathsf{con}}^{T} \Psi\right] - E \left[\Psi^{T}\right] C_{\mathsf{con}} C_{\mathsf{con}}^{T} E[\Psi]\right)}_{S} A_{eq} U \tag{41}$$

 $\forall \tilde{k}$. Defining a new matrix S (S is real symmetric positive semidefinite) in (41), we can derive

$$\operatorname{var}\left[C_{\operatorname{con}}^{T}Z\left(\tilde{k}\right) - 0.15\right]^{1/2} = \left|\left|\Lambda^{1/2}V^{T}A_{eq}U\right|\right|_{2} \tag{42}$$

where an SVD decomposition of S is done as, $S = V\Lambda V^T$. Once again, the matrices comprising expected values ($E[\Psi]$ and S) are distribution dependent. Finally, the constraints described in (32) and (33) can be summarized by the convex constraints

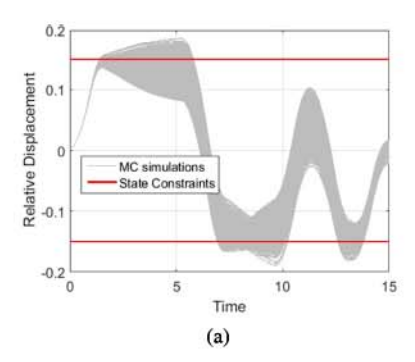
$$k_e \left| \left| \Lambda^{1/2} V^T A_{eq} U \right| \right|_2 + C_{\mathsf{con}}^T E[\Psi] A_{eq} \left(\tilde{k} \right) U - 0.15 \le 0,$$

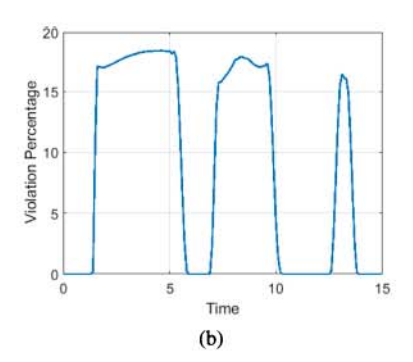
$$k_e \left| \left| \Lambda^{1/2} V^T A_{eq} U \right| \right|_2 - C_{\mathsf{con}}^T E[\Psi] A_{eq} \left(\tilde{k} \right) U - 0.15 \le 0.$$

$$(43)$$

Equation (43) is used to enforce the state constraints when solving for U.

Fig. 5(a) shows a plot with the MC realizations of the relative displacement (for $\epsilon_1 = 0.5$, i.e., for a 50% constraint violation allowance). It presents results for the case of the beta distributed





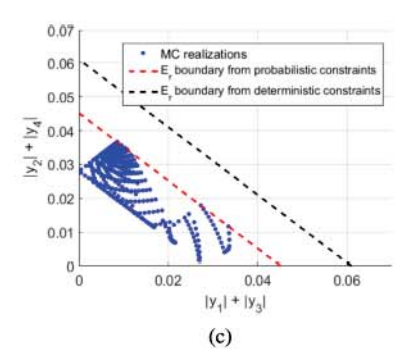


Fig. 5. (a) Relative displacement versus time for probabilistic state constraint. (b) Percentage violation versus time. (c) Residual energy plot.

TABLE I
COMPARISON ACROSS DISTRIBUTIONS FROM 100 000 MC SIMULATIONS

	Uniform		Beta		Custom	
ϵ_1	f	Max. V	f	Max. V	f	Max. V
0.2	0.0388	4.92	0.0516	5.85	0.0651	5.67
0.5	0.0316	20.71	0.0451	18.39	0.0596	17.31
0.8	0.0287	34.77	0.0424	34.43	0.0572	33.59

r.v. [i.e., when k and c are given by (26)]. It can be seen that the state constraints are in fact violated. Fig. 5(b) shows the percentage of times these violations take place from 100 000 simulations.

Although a 50% violation was allowed, a maximum violation of only 18.39% is observed. This is not an anomaly, since we must remember that the probabilistic constraint is a conservative one and that the violations are a function of the distribution. Table I presents the different maximum percentage violations (Max. V) that were observed for the three distributions.

Another interesting observation about the results can be made from the optimal value of the cost (i.e., f). For a Level 0 approximation E_r , in the deterministic case (where state constraints are nonprobabilistic) the cost f is seen to be 0.0610; while the probabilistic case with a beta distribution is seen to have a cost of 0.0451 [Fig. 5(c)]. It should be noted that the x-axis and the y-axis correspond to the measures of the violations of the states associated with the first and second masses, respectively, from the desired terminal states. The dashed black line is the energy bound determined from the deterministic problem formulation. The red dashed line is the residual energy bound corresponding to the case where the state constraints are probabilistic and the terminal energy constraint is deterministic. The blue dots represent the components of the terminal residual energy for every realization of the MC simulations.

A lower cost for the probabilistic state constraints is expected since a probabilistic constraint is not a hard one. Therefore, if certain violations are allowed, the final residual energy cost is bound to improve. This trend of decreasing optimal cost with the increased probability constraint violations can be seen across all distributions (see Table I).

C. Probabilistic State and Energy Constrained Solution

This section is used to present the results for the floating oscillator maneuver when the optimization problem (P4) is solved.

An approach similar to the probabilistic state constraints is used to enforce the probabilistic terminal residual energy constraint. Since, the formulation only allows for linear constraints, only the linear versions of the residual energy (see Section III-A) can be incorporated.

Therefore, in this section, (P4) is solved with the probabilistic state constraints [same as (32) and (33)] and the probabilistic Level 0 residual energy constraints

$$Prob\{\pm y_1 \pm y_2 \cdots \pm y_{\tilde{n}} - f \le 0\} \ge 1 - \epsilon_2$$
 (44)

where y_i are defined through (11). It should be noted that (44) represents a total of 16 constraints for the fourth-order system. The control constraints are chosen to be the same as before, given by (23).

 y_i has been explicitly expanded for the example problem in the following equations:

$$y_1 = K_1 C_k (Z(T_f) - Z_d(T_f))$$
 (45)

$$y_2 = K_2 C_k (Z(T_f) - Z_d(T_f))$$
 (46)

$$y_3 = M_1 C_m (Z(T_f) - Z_d(T_f))$$
 (47)

$$y_4 = M_2 C_m (Z(T_f) - Z_d(T_f))$$
 (48)

where $\sqrt{K} = [K_1^T, K_2^T]^T, \sqrt{M} = [M_1^T, M_2^T]^T$

$$C_k = \begin{bmatrix} 1 & 0 & 0 & 0 \\ 0 & 1 & 0 & 0 \end{bmatrix}, \ C_m = \begin{bmatrix} 0 & 0 & 1 & 0 \\ 0 & 0 & 0 & 1 \end{bmatrix}. \tag{49}$$

One must remember that K_1 and K_2 are still random row vectors since K is a random matrix. The development of just one of the constraints is shown. The other constraints can be derived in an identical fashion. The constraint shown is

$$Prob\{y_1 + y_2 + y_3 + y_4 - f \le 0\} \ge 1 - \epsilon_2. \tag{50}$$

Similar to the previous section, (50) is equivalent to

$$k_e \{ \text{var}[C_{\text{con2}}Y - f] \}^{1/2} + E[C_{\text{con2}}Y - f] \le 0$$
 (51)

where
$$k_e = \sqrt{\frac{1-\epsilon_2}{\epsilon_2}}$$
 and $C_{\mathsf{con2}} = [1, 1, 1, 1]$.

Now,
$$E[C_{con2}Y - f] = C_{con2}E[Y] - f$$

$$= C_{con2} \begin{bmatrix} E[K_1C_kZ(T_f) - K_1C_kZ_d(T_f)] \\ E[K_2C_kZ(T_f) - K_2C_kZ_d(T_f)] \\ E[M_1C_mZ(T_f) - M_1C_mZ_d(T_f)] \\ E[M_2C_mZ(T_f) - M_2C_mZ_d(T_f)] \end{bmatrix} - f. \quad (52)$$

But on substituting $Z(T_f) = \Psi A_{eq}(\bar{k}_f)U$ (where \tilde{k}_f is the final time iteration number), (52) can be written as

$$E[C_{con2}Y - f] =$$

$$C_{\text{con2}}\underbrace{\begin{bmatrix} E[K_1C_k\Psi]A_{eq}(\tilde{k}_f)U - E[K_1]C_k\boldsymbol{Z_d}(T_f) \\ E[K_2C_k\Psi]A_{eq}(\tilde{k}_f)U - E[K_2]C_k\boldsymbol{Z_d}(T_f) \\ E[M_1C_m\Psi]A_{eq}(\tilde{k}_f)U - M_1C_m\boldsymbol{Z_d}(T_f)] \\ E[M_2C_m\Psi]A_{eq}(\tilde{k}_f)U - M_2C_m\boldsymbol{Z_d}(T_f)] \end{bmatrix}}_{E_y} - f.$$

Moreover,

$$\operatorname{var}[C_{\operatorname{con2}}Y - f] = \operatorname{var}[C_{\operatorname{con2}}Y] = C_{\operatorname{con2}}\operatorname{var}[Y]C_{\operatorname{con2}}^{T}$$
 (53)

since f is simply a number and not a r.v. Equation (53) can be simplified to

$$\operatorname{var}[C_{\operatorname{con2}} Y - f] = C_{\operatorname{con2}} \left\{ E \left[Y Y^T \right] - E \left[Y \right] E \left[Y \right]^T \right\} C_{\operatorname{con2}}^T. \tag{54}$$

After the substitution of Y and some algebraic manipulations we get

$$var[C_{con2}Y] = U^T P U + 2Q U + R$$
(55)

where

$$P = A_{eq} \left(\tilde{k}_f \right)^T \left(E \left[\Psi^T L^T C_{\text{con2}}^T C_{\text{con2}} L \Psi \right]$$

$$- E \left[\Psi^T L^T \right] C_{\text{con2}}^T C_{\text{con2}} E[L \Psi] \right) A_{eq} \left(\tilde{k}_f \right)$$

$$Q = \mathbf{Z_d}^T \left(E[L]^T C_{\text{con2}}^T C_{\text{con2}} E[L \Psi]$$

$$- E \left[L^T C_{\text{con2}}^T C_{\text{con2}} L \Psi \right] \right) A_{eq} \left(\tilde{k}_f \right)$$
 and (57)
$$R = \mathbf{Z_d}^T \left(E \left[L^T C_{\text{con2}}^T C_{\text{con2}} L \right]$$

$$- E[L^T] C_{\text{con2}}^T C_{\text{con2}} E[L] \right) \mathbf{Z_d}.$$
 (58)

L is defined in (11). Since, $var[C_{con2}Y] \ge 0$, a factorization exists of the form

$$var[C_{con2}Y] = (MU+D)^T(MU+D)$$
(59)

(58)

in which case we get

$$var[C_{con2}Y - f]^{1/2} = ||MU + D||_2.$$
 (60)

Therefore, the probability constraint [see (50)] finally becomes the convex constraint

$$k_e||MU + D||_2 + C_{\text{con}2}E_v - f \le 0.$$
 (61)

The other probability constraints to enforce the residual energy can be done in the same way [from a development similar to (50) through (61)].

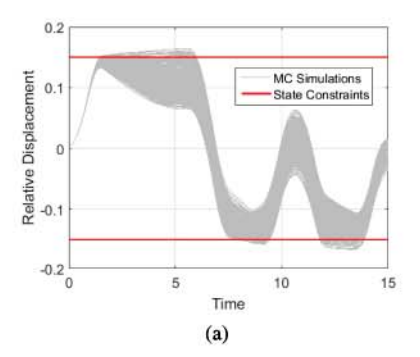
After the formulation of all the constraints (both the state and terminal residual energy), the optimization problem was solved. Results for only one of the cases (case with the beta distributed r.v. and a Level 0 approximation of the residual energy) is presented. Fig. 6(a) shows a plot with the MC realizations of the relative displacement (for $\epsilon_1 = 0.2$ and $\epsilon_2 = 0.5$) where it is seen that the state constraints are violated again. Fig. 6(b) provides an estimate of the percentage of the times; these constraints were violated for 100 000 MC simulations. Since, the constraints are all conservative, a maximum violation of only 5.65% is observed (although the allowance was 20%).

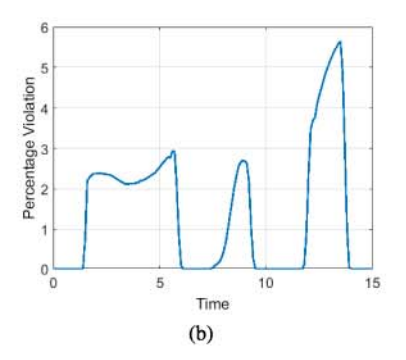
Fig. 6(c) shows a plot of the residual energy. The red dotted line indicates the cost determined for the case of probabilistic state and energy constraints. The black dotted line is the deterministic counterpart and is the same as Fig. 5(c). It can be seen that the cost (f = 0.0221) has significantly reduced since the constraints are no longer hard (as limited violations are permitted) compared to the deterministic case (f = 0.0610). Furthermore, it is seen that the cost is less even compared to when only state constraints were probabilistic (f = 0.0516 for $\epsilon_1 = 0.2$ in Table I) as expected. The blue dots represent the MC realizations when both the constraints (state and energy) are probabilistic. From the 100 000 MC simulations [used to generate Fig. 6(a)–(c)], the Max. V of an energy constraint was estimated to be 17.33% (well within the allowed 50%). This means that the majority of the blue dots lie within the red dotted line.

The violations are all distribution dependent and Table II has been used to list the results for the three distributions for the various combinations of ϵ_1 and ϵ_2 , all assuming a Level 0 approximation of the residual energy. Max. V_s and Max. V_e represents the maximum violations observed for any state and energy constraint, respectively. Similar results were noted when a Level 1 approximation for the residual energy was exercised.

We observe consistently that the cost is better with a Level 1 approximation as compared to a Level 0 approximation of E_r . It should be noted that this observation is not a guarantee for all problems. It is highly dependent on the nature of the variation of E_r with respect to the uncertain parameters. However, a higher level approximation pushes the solution towards the true residual energy (which is quadratic in x space) solution.

Fig. 7 presents a color coded plot of the three distributions considered in the design of the chance-constrained controllers. The first row of the graphs represent a plan view of the pdfs with the regions of the compact support marked in blue and red to illustrate the regions of the uncertain domain that satisfy and those that violate the residual energy constraint, respectively. The second row presents the three distributions from a view point that illustrate the shape of the pdf in conjunction with the regions demarcated to illustrate the domain which satisfies the chance constraint. For the uniform distribution (first column) the region which corresponds to a smaller damping constant is associated with the violation of the residual energy bound. This trend is seen in the other two distributions as well.





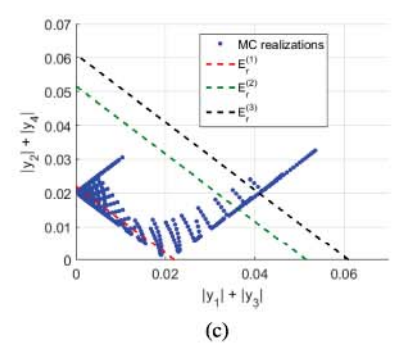


Fig. 6. (a) Relative displacement versus time for probabilistic state and energy constraint. (b) Percentage violation versus time. (c) Residual energy boundary: $E_r^{(1)}$: Probabilistic state and energy constraints, $E_r^{(2)}$: Probabilistic state constraints, $E_r^{(3)}$: Deterministic state and energy constraints.

TABLE II COMPARISON ACROSS DISTRIBUTIONS FROM 100 000 MC SIMULATIONS (LEVEL 0 E_r APPROXIMATION)

ϵ_1 ϵ_2		Uniform			Beta		Custom			
	ϵ_2	f	Max. V _s	Max. V _e	f	Max. V _s	Max. V _e	f	Max. V_s	Max. Ve
0.2	0.2	0.0347	5.64	5.41	0.0355	6.02	5.77	0.0361	5.76	5.59
0.2	0.5	0.0217	4.80	20.11	0.0221	5.65	17.33	0.0223	5.56	16.23
0.2	0.8	0.0126	4.16	42.43	0.0128	5.27	40.86	0.0129	5.34	40.00
0.5	0.2	0.0273	20.75	6.28	0.0286	18.31	6.10	0.0295	17.03	5.71
0.5	0.5	0.0162	20.77	18.96	0.0168	18.32	16.09	0.0172	17.41	15.09
0.5	0.8	0.0090	20.86	44.47	0.0093	18.38	41.76	0.0095	17.16	40.05
0.8	0.2	0.0242	34.89	6.36	0.0258	34.44	6.12	0.0269	34.09	5.70
0.8	0.5	0.0140	34.41	17.94	0.0147	34.52	15.30	0.0153	33.99	14.28
0.8	0.8	0.0077	34.62	42.51	0.0081	34.31	39.93	0.0083	33.92	36.90

However, it can be noted that in the nonuniform pdfs, as the high probability regions (around the mean of the k-c space), gets more prominent, larger regions of the periphery of the uncertain domain (which correspond to the low probability regions) are represented to a greater degree in the red region. Given that the geometry of the region of the uncertain domain which corresponds to the satisfaction of the chance constraint is complex, a sampling-based approach would be very expensive (albeit less conservative) to determine the optimal controller. This is in contrast to the convex optimization problem posed with the chance constraint, which is only dependent of the mean and variance of the states which can be easily determined by the PC expansion.

V. EXPERIMENTAL RESULTS

A Quanser-coupled two-tank system is used to experimentally validate the performance of the proposed chance-constrained controller. The specifications can be found on the website link in [22].

The coupled tank setup was connected to a Quanser Universal Power Module (UPM-15-03) for signal amplification. Data acquisition was accomplished on a Windows PC (Dell Optiplex 7020) via a Quanser NI E-Series Terminal Board with the help of a National Instruments Data Acquisition Card (NI PCI 6221). The coupled tank system has integrated pressure/level sensors configured for each tank. Water level measurements were acquired from these sensors using the aforementioned setup. Quanser real-time control software (Quarc) along with MATLAB/Simulink was used to implement the controllers and process measurement data.

It should be noted that the pump/motor dynamics are much faster than the water level dynamics and therefore have been factored out of the control design. The chance constraint algorithm proposed in this paper is for linear systems while, the cascaded 2 tank model is an inherently nonlinear one given by equations

$$\dot{z}_2 = -a_1 \sqrt{2g} \sqrt{z_2} / A_1 + k V_m / A_1 \tag{62}$$

$$\dot{z}_3 = -a_2\sqrt{2g}\sqrt{z_3}/A_2 + a_1\sqrt{2g}\sqrt{z_2}/A_2 \tag{63}$$

where z_2 and z_3 denote the levels of the upper and the lower tank, respectively. The corresponding areas of the tanks are A_1 and A_2 while the effluent areas are denoted by a_1 and a_2 . The gravity is denoted by g, the voltage to input flow conversion constant by k and the applied voltage to the pump by V_m . Therefore, in this experiment the nonlinearities of the system will be characterized by the uncertainties in parameters of a linearized model. The model is linearized about a certain equilibrium operating point $([z_2, z_3]^T$ and V_m) to yield the linear dynamics in the perturbation space as

$$\begin{bmatrix} \delta \dot{z}_2 \\ \delta \dot{z}_3 \end{bmatrix} = \begin{bmatrix} \frac{-a_1\sqrt{2g}}{2\sqrt{z_2}A_1} & 0 \\ \frac{a_1\sqrt{2g}}{2\sqrt{z_3}A_2} & \frac{-a_2\sqrt{2g}}{2\sqrt{z_3}A_2} \end{bmatrix} \begin{bmatrix} \delta z_2 \\ \delta z_3 \end{bmatrix} + \begin{bmatrix} k/A_1 \\ 0 \end{bmatrix} \delta V_m. \tag{64}$$

Based on this linearized model, defining the parameters $p_1=k/A_1,\ p_2=\frac{a_1\sqrt{2g}}{2\sqrt{z_2}A_1}$, $p_3=\frac{a_1\sqrt{2g}}{2\sqrt{z_2}A_2}$, and $p_4=\frac{a_2\sqrt{2g}}{2\sqrt{z_3}A_2}$ yields the transfer functions defined by S_1 and S_2 in Fig. 8. A transfer function block diagram of the system is illustrated in Fig. 8 which includes a proportional integral (PI) controller. S_1 and S_2 are the 1st-order transfer functions mapping the change in motor voltage (δV_m) to the change in the water level in Tank

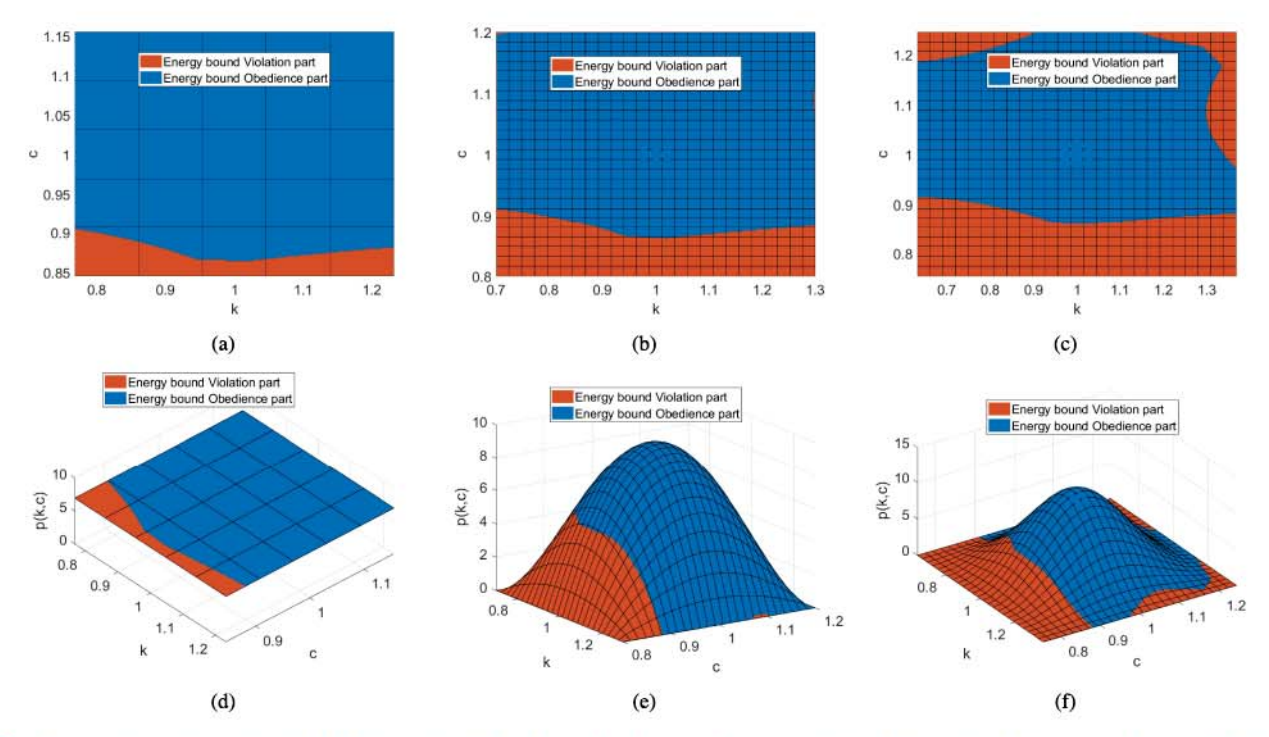


Fig. 7. Region of uncertain domain that does not satisfy the residual energy chance constraint shown in red (for $\epsilon_1 = 0.2$, $\epsilon_2 = 0.2$). (a) and (d) Uniform distribution. (b) and (e) Beta distribution. (c) and (f) Custom distribution.

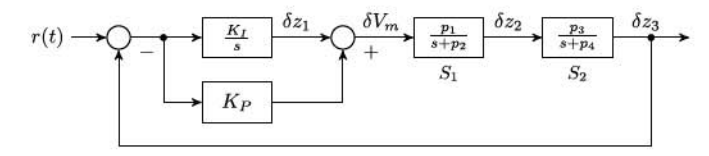


Fig. 8. Block diagram of system.

 $1 [\delta z_2(t)]$ and the change in the water level in the Tank 1 to the change in the water level in the Tank 2 $[\delta z_3(t)]$, respectively. The operating point is indicated by V_m , the motor voltage at which the system is at equilibrium which serves as a surrogate for the water levels in the tank at the steady-state.

Therefore, S_1 and S_2 (i.e., the parameters p_1 through p_4) were identified separately for the different values of $V_m \in [4.2, 5.8]$. This was done by applying a constant V_m to the pump, allowing the system to reach an equilibrium $([z_2, z_3])$, then applying a constant voltage of $(V_m + \delta V_m)$ and observing the step response of the change in the water level of the tanks $([\delta z_2(t), \delta z_3(t)])$. Hence, p_1 through p_4 were calculated as a function of the operating point V_m .

For illustrating the chance-constraint approach, it is assumed that the operating point (V_m) is uncertain (with a uniform distribution U[4.2,5.8]) and that the system model is a function of this uncertain variable. The state-space representation of the block diagram represented in Fig. 8 is given by

$$\begin{bmatrix} \dot{\delta}z_{1} \\ \dot{\delta}z_{2} \\ \dot{\delta}z_{3} \end{bmatrix} = \underbrace{\begin{bmatrix} 0 & 0 & -K_{I} \\ p_{1} & -p_{2} & -p_{1}K_{P} \\ 0 & p_{3} & -p_{4} \end{bmatrix}}_{A} \underbrace{\begin{bmatrix} \delta z_{1} \\ \delta z_{2} \\ \delta z_{3} \end{bmatrix}}_{Z} + \underbrace{\begin{bmatrix} K_{I} \\ p_{1}K_{P} \\ 0 \end{bmatrix}}_{B} r(t)$$
(65)

where $K_P=1$ and $K_I=0.03$ were chosen as the PI controller gains. The objective of the design problem is to determine a reference trajectory r(t) which transitions the above system from the initial equilibrium position $Z(0)=[0,0,0]^T$ to the desired equilibrium $Z_{\mathbf{d}}(T_f=50)=-A^{-1}B$ (which effectively raises the Tank 2 water level by 1 unit) at final time (T_f) irrespective of the operating point V_m . Control constraints of the form $\delta V_m(t) \leq 2$ and $\delta V_m(t) \geq -1$ are also imposed. Following the development previously explained, a set of residual states are defined as $X=Z_{\mathbf{d}}(T_f)-Z(T_f)$. Assuming a l_∞ linear formulation for the associated residual energy ([similar to (14)], a new set of states Y=X [similar to (11)] is used to enforce the residual energy constraints [i.e., $E_r=\max(|Y|)$].

The chance constraint control solution [i.e., solution to (P4)] is then obtained using the methodology outlined in the flowchart. It should be noted that there are no state constraints in the problem and therefore the chance constraints were only enforced on the terminal constraints. The percentage of violation allowed was limited to 10%. A nominal model control solution was obtained by determining the control trajectory for the operating point $V_m = 0.5 \ (4.2 + 5.8)$. The worst case scenario control was obtained by solving the minimax optimization problem (P2) where the uncertain space of V_m was uniformly sampled.

The control solutions were then applied to 52 operating points (V_m) distributed in the uncertain domain and Y for each case was recorded. Fig. 9 shows the variation of the residual energy for each control algorithm with respect to the uncertain variable. It is clear that the control derived from the nominal model performs poorly as one moves away from the nominal operating point. A significant difference, on the other hand, is visually not clear between the worst case and the chance-constraint-based design.

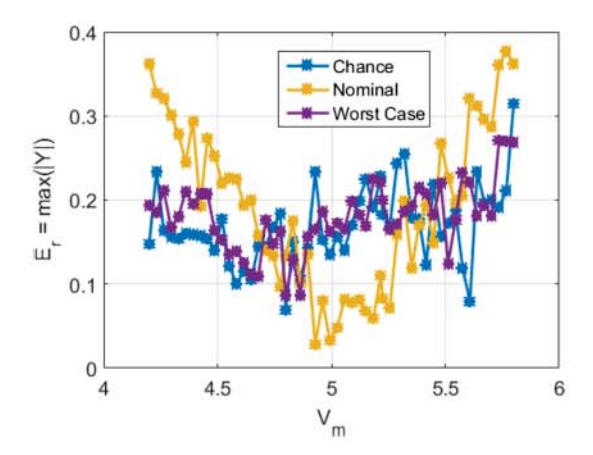


Fig. 9. Variation of the residual energy with V_m .

TABLE III
STATISTICS ON THE OBSERVED RESIDUAL ENERGIES

Controller	Chance Constraint	Nominal	Worst Case	
$Mean(E_r)$	0.1692	0.1925	0.1797	
$Variance(E_r)$	0.0022	0.0096	0.0017	
$max(E_r)$	0.2335*	0.3772	0.2704	

^{*} The maximum is computed after removing the top 10% of the E_r values.

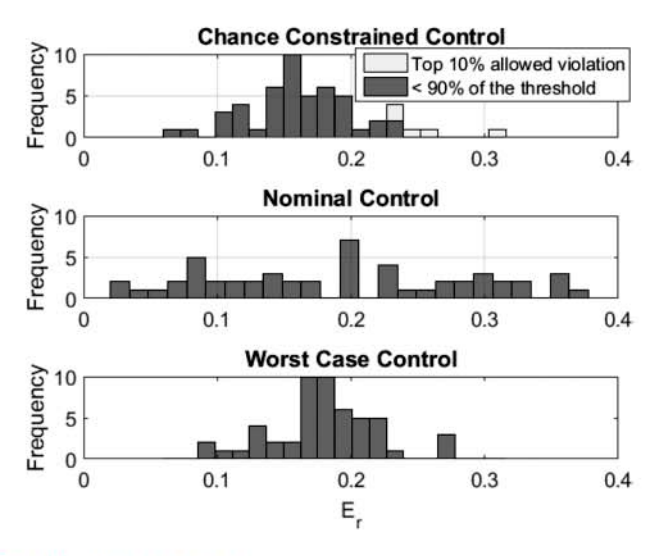


Fig. 10. Histograms of E_r .

However, on calculating the mean residual energy of all the algorithms (see Table III), it can be seen that the chance-constraint-based design outperforms the others. In fact, an improvement of 12.1% with respect to the nominal mean E_r is observed for the chance constrained mean E_r (as compared to a 6.7% improvement for the worst case mean E_r). Furthermore, an improvement of 38.10% is observed for the chance constrained control when compared to the maximum value of the nominal control E_r (as compared to a 28.31% improvement for the worst case control). Fig. 10 shows a histogram plot of the 52 residual energies that were obtained from the experiment. The nominal control plot shows the worst performance with several residual energies seen beyond the $E_r = 0.25$ mark. The worst case design performs reasonably well with only a single occurrence of $E_r > 0.25$. However, the chance constrained control (on remov-

ing the top 10%) shows no value of $E_r > 0.25$. Furthermore, the mean E_r for chance-constrained control is lower than the worst case counterpart (even after including the top 10%); thereby showing that if a modicum number of violations are acceptable, the chance-constrained methodology provides a more robust performance.

VI. CONCLUSION

This paper presented a convex optimization formulation for the design of controllers for linear systems with the model parameter uncertainties. The probabilistic representation of the model parameter uncertainties is suited to the use of PC to convert the stochastic model to a deterministic surrogate model, which permits evaluation of the mean and variance of the evolving states. The chance constraints are used to formulate a convex optimization problem as a function of an acceptable level of the constraint violation. Since the problem formulation is agnostic to the distribution of the uncertainty if their mean and variance match, three distributions are selected to illustrate the relative performance for the benchmark floating oscillator problem. It is seen that the constraint violation is always significantly smaller than the bounds that are imposed in the optimal control problem. Experimental results on a coupled two-tank system help illustrate the benefits of the chance-constrained design approach relative to a nominal control and worst case design.

ACKNOWLEDGMENT

All results and opinions expressed in this paper are those of the authors and do not reflect opinions of NSF.

REFERENCES

- N. C. Singer and W. P. Seering, "Preshaping command inputs to reduce system vibration," J. Dyn. Syst., Meas., Control, vol. 112, no. 1, pp. 76–82, 1990
- [2] T. Oomen, "Advanced motion control for precision mechatronics: Control, identification, and learning of complex systems," *IEEJ J. Ind. Appl.*, vol. 7, no. 2, pp. 127–140, 2018.
- [3] S. Nandi, V. Migeon, T. Singh, and P. Singla, "State constrained controller design for uncertain linear systems using polynomial chaos," in *Proc. IEEE Amer. Control Conf.*, 2016, pp. 2005–2010.
- [4] S. Devasia, E. Eleftheriou, and S. R. Moheimani, "A survey of control issues in nanopositioning," *IEEE Trans. Control Syst. Technol.*, vol. 15, no. 5, pp. 802–823, Sep. 2007.
- [5] J. Park, P.-H. Chang, H.-S. Park, and E. Lee, "Design of learning input shaping technique for residual vibration suppression in an industrial robot," *IEEE/ASME Trans. Mechatron.*, vol. 11, no. 1, pp. 55–65, Feb. 2006.
- [6] H. Moradi, M. Saffar-Avval, and F. Bakhtiari-Nejad, "Sliding mode control of drum water level in an industrial boiler unit with time varying parameters: A comparison with h-robust control approach," J. Process Control, vol. 22, no. 10, pp. 1844–1855, 2012.
- [7] T. Singh and S. Vadali, "Robust time-delay control," J. Dyn. Syst., Meas., Control, vol. 115, no. 2A, pp. 303–306, 1993.
- [8] T. Singh, "Minimax design of robust controllers for flexible systems," J. Guid., Control, Dyn., vol. 25, no. 5, pp. 868–875, 2002.
- [9] G. Schildbach, G. C. Calafiore, L. Fagiano, and M. Morari, "Randomized model predictive control for stochastic linear systems," in *Proc. IEEE Amer. Control Conf.*, 2012, pp. 417–422.
- [10] G. Schildbach, P. Goulart, and M. Morari, "The linear quadratic regulator with chance constraints," in *Proc. Eur. Control Conf.*, 2013, pp. 2746–2751.

- [11] K.-K. K. Kim and R. D. Braatz, "Generalised polynomial chaos expansion approaches to approximate stochastic model predictive control," *Int. J. Control*, vol. 86, no. 8, pp. 1324–1337, 2013.
- [12] G. C. Calafiore and L. El Ghaoui, "On distributionally robust chanceconstrained linear programs," J. Optim. Theory Appl., vol. 130, no. 1, pp. 1–22, 2006.
- [13] A. Mesbah, S. Streif, R. Findeisen, and R. D. Braatz, "Stochastic nonlinear model predictive control with probabilistic constraints," in *Proc. IEEE Amer. Control Conf.*, 2014, pp. 2413–2419.
- [14] N. Wiener, "The homogeneous chaos," Amer. J. Math., vol. 60, no. 4, pp. 897–936, 1938. [Online]. Available: http://www.jstor.org/ stable/2371268
- [15] D. Xiu and G. E. Karniadakis, "The wiener-askey polynomial chaos for stochastic differential equations," SIAM J. Sci. Comput., vol. 24, no. 2, pp. 619-644, Feb. 2002. [Online]. Available: http://dx.doi.org/ 10.1137/S1064827501387826
- [16] S. Garatti and M. C. Campi, "Modulating robustness in control design: Principles and algorithms," *IEEE Control Syst.*, vol. 33, no. 2, pp. 36–51, Apr. 2013.
- [17] B. Wie and D. S. Bernstein, "Benchmark problems for robust control design," J. Guid., Control, Dyn., vol. 15, no. 5, pp. 1057–1059, 1992.
- [18] T. Singh, "Minimax input shaper design using linear programming," J. Dyn. Syst., Meas., Control, vol. 130, no. 5, 2008, Art. no. 051010.
- [19] H. N. Najm, "Uncertainty quantification and polynomial chaos techniques in computational fluid dynamics," *Annu. Rev. Fluid Mech.*, vol. 41, pp. 35– 52, 2009.
- [20] T. Singh, P. Singla, and U. Konda, "Polynomial chaos based design of robust input shapers," J. Dyn. Syst., Meas., Control, vol. 132, no. 5, 2010, Art. no. 051010.
- [21] K.-K. K. Kim, D. E. Shen, Z. K. Nagy, and R. D. Braatz, "Wiener's polynomial chaos for the analysis and control of nonlinear dynamical systems with probabilistic uncertainties [historical perspectives]," *IEEE Control Syst.*, vol. 33, no. 5, pp. 58–67, Oct. 2013.
- [22] "Quanser-coupled-tanks-system-datasheet." [Online]. Available: https:// www.quanser.com/products/coupled-tanks/. Accessed on: 2018-01-03.



Souransu Nandi (S'17) received his B.Tech degree in electrical engineering from NIT Durgapur, Durgapur, India, in 2014.

He is currently working toward his Ph.D. degree at the University at Buffalo, Buffalo, NY, USA. His research interests include uncertainty quantification, estimation, and control.



Tarunraj Singh (SM'17) received the B.E. degree from Bangalore University, Bangalore, India, in 1986, the M.E. degree from the Indian Institute of Science, Bangalore, India, in 1988 and the Ph.D. degree from the University of Waterloo, Waterloo, ON, Canada, in 1991, all in mechanical engineering.

Since 1993, he has been with the University at Buffalo, Buffalo, NY, where he is currently a Professor with the Department of Mechanical and Aerospace Engineering. His research

interests include robust vibration control, estimation, and uncertainty quantification.